11th World Congress on Computational Mechanics (WCCM XI)
5th European Conference on Computational Mechanics (ECCM V)
6th European Conference on Computational Fluid Dynamics (ECFD VI)
E. Oñate, J. Oliver and A. Huerta (Eds)

INVESTIGATION OF A BUBBLE ATTACHED AND SLIDING ON A CYLINDER

BAOYU NI*

*College of Shipbuilding Engineering, Harbin Engineering University
Harbin 150001, P.R. China
e-mail:baoyuni@gmail.com, www.hrbeu.edu.cn

Key Words: *Bubble Dynamics, Moving Boundary, Drag Reduction, Boundary Element Method.*

Abstract. The evolution and dynamics of a bubble attached and sliding on an axisymmetric cylinder is simulated and analyzed based on velocity potential theory. The intersection points of the bubble and the body are treated specially by the numerical technique and a widely applicable code is obtained based on Boundary Element Method (BEM). The variation of the bubble pressure with its volume is taken into account. Fully nonlinear dynamic and kinematic conditions are imposed on the bubble surface. A typical case is studied and the dynamic responses of the bubble, body and the flow field are simulated. The effects of initial bubble volume on the interactions are investigated. It is aimed that the results from this paper would provide some insight into the drag reduction on marine vehicles through using bubbles and air cavity.

1 INTRODUCTION

When a vehicle moves forwards in a liquid, such as water, it will encounter much larger drag than it does in the air, because the former has much larger density. Therefore there is always a strong desire to reduce the drag through introducing bubbles or air cavity over the body surface. In fact there has been a large body of work in this area. In terms of their mechanisms, drag reduction through bubble could be broadly classified as Micro-Bubble Drag Reduction (MBDR or BDR) and Air Layer Drag Reduction (ALDR), which were reviewed by Ceccio (2010)[1]. MBDR reduces the frictional resistance by forming the micro bubble-water mixed layer on the bottom surface of the body. This concept was first demonstrated by McCormick & Bhattacharyya (1973)[2], who studied the drag reduction of an axisymmetric body through hydrogen bubbles generated by electrolyzing water. ALDR reduces the frictional drag by covering parts of the hull surface of the vehicle with an air layer (also known as air cavity, ventilated cavity, or air plenum), which effectively reduces the wetted area of the body surface (Latorre, 1997)[3]. Subsequently, a series mathematical analyses and numerical simulations have been undertaken to assess the feasibility of these two concepts, and to refine and improve both technologies.

In mathematical modelling and numerical simulations, the underlying mechanism of bubble drag reduction has always been an active topic of research. For MBDR, research is

based mainly on two approaches: one is the boundary layer theory, which considers the fluid as a homogeneous mixture with reduction in density and modification of the effective viscosity inside the boundary layer (Legner, 1984[4]; Madavan et al., 1985[5]) and the other is two-phase flow theory (Brockett, 1969[6], Drew, 1983[7]). Many numerical simulations have been based on these two approaches over the past decades and a review can be found in Ceccio (2010)[1]. By contrast, fewer investigations have been conducted for the ALDR phenomenon. Matveev (1999)[8] developed a simplified model of a two-dimensional cavity based on the potential flow theory, which was then extended to three-dimensional problems (Matveev 2009[9]). Li et al. (2008)[10] used a two-dimensional air cavity formation for a slender ship and then examined the parameters which directly affected the formation of air cavities, such as cavitation number and ship speed. Choi et al. (2005[11], 2010[12]) studied the deformation of the air layer beneath a ship hull and considered its effects on wave making resistance with the three-dimensional boundary element method. Some insights into the problem have been obtained in the studies of Choi et al. (2005[11], 2010[12]), but the air-liquid interface is treated as a cavity surface with fixed end nodes at the edges of the ship plenum cavity. An advantage of this approach is that it avoids complicated regrinding on the hull surface and therefore saving the computation time. However its disadvantage is the slide of air-liquid surface along the hull cannot be simulated directly due to the fixed end nodes. Ni et al.(2013) erected a numerical model of a ring bubble attached on an ellipsoid, and studied the motion and deformation of the bubble along the ellipsoid. The convergence study is undertaken to assess the developed numerical method and the computation code. On this basis, the effects of initial bubble pressure and initial bubble release position are investigated. This paper is the extension of Ni et al.(2013), which shall principally focus on the effects of initial bubble volume as well as the surface tension.

2 MATHEMATICAL MODEL

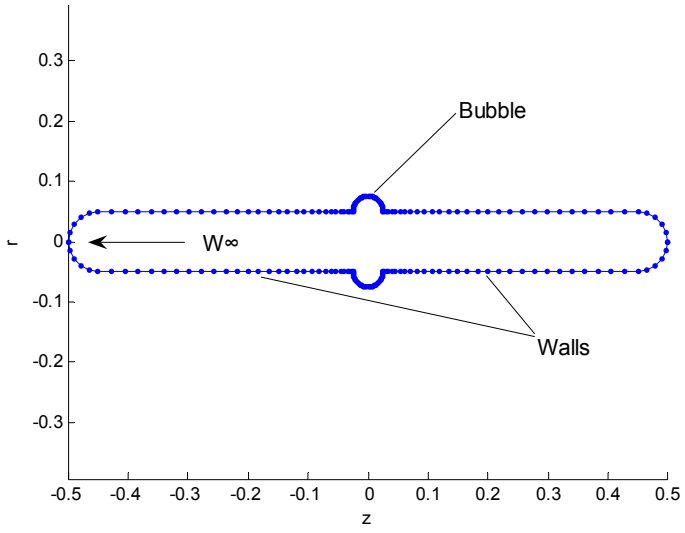

Figure 1: Sketch of the problem (longitudinal profile)

Fig.1 gives a longitudinal profile of the problem to be considered, which shows a body of

resolution with an attached bubble moving forward with W_∞ in the unbounded fluid domain. The gravity effect on the bubble is ignored and the flow is assumed to be axisymmetric. We further assume that the fluid is inviscid and incompressible, and the flow is irrotational. Therefore, the velocity potential Φ can be introduced and velocity vector follows $\boldsymbol{u} = \nabla\Phi$. When it is coupled with continuity equation $\nabla \cdot \boldsymbol{u} = 0$, Laplace's equation can be obtained for the potential:

$$\nabla^2\Phi = 0 \tag{1}$$

in the fluid domain. The boundary condition on the rigid body surface is given by

$$\frac{\partial\Phi}{\partial n} = \boldsymbol{W}_\infty \cdot \boldsymbol{n} \tag{2}$$

where $\boldsymbol{n}$ is the inward normal vector of the body surface. Furthermore, in the Lagrangian framework, the fully nonlinear kinematic and dynamic boundary conditions on the bubble surface can be written as

$$\frac{d\boldsymbol{r}}{dt} = \nabla\Phi \tag{3}$$

$$\frac{d\Phi}{dt} - \frac{1}{2}|\nabla\Phi|^2 + \frac{P_l}{\rho} = \frac{P_\infty}{\rho} \tag{4}$$

where $\boldsymbol{r} = (r, \theta, z)$ is the position vector of the fluid particle on the bubble surface, d/dt is the substantial derivative, ρ is the density of the liquid, P_∞ is the ambient pressure at infinite and P_l is the fluid pressure on the bubble surface.

It is assumed that the bubble here contains non-condensable gas only, which is assumed to satisfy a polytropic law with an exponent τ. The surface tension is also considered here, so the pressure on the bubble surface is:

$$P_l = P_0\left(\frac{V_0}{V}\right)^\tau - \sigma\nabla \cdot \boldsymbol{n} \tag{5}$$

where P_0 and V_0 are the initial gas pressure inside and volume when the bubble is formed, τ is the ratio of specific heat of the gas, σ is the surface tension, $\nabla \cdot \boldsymbol{n}$ is the local surface curvature.

Substituting Eq. (5) into Eq.(4), we obtain the dynamic condition on the bubble surface in Lagrangian framework as follow:

$$\frac{d\Phi}{dt} = \frac{1}{\rho}\left\{P_\infty - \left(P_0\left(\frac{V_0}{V}\right)^\tau - \sigma\nabla \cdot \boldsymbol{n}\right)\right\} + \frac{1}{2}|\nabla\Phi|^2 \tag{6}$$

Finally, the boundary condition at infinity is:

$$\Phi \to 0 \qquad (\boldsymbol{r} \to \infty) \tag{7}$$

By using Green's third identity and the Green function *G*, the velocity potential at a field point $\boldsymbol{m}$ in the fluid can be represented by

$$\varepsilon\Phi(\boldsymbol{m}) = \iint_S \left(\frac{\partial \Phi(\boldsymbol{l})}{\partial n} G(\boldsymbol{m},\boldsymbol{l}) - \Phi(\boldsymbol{l}) \frac{\partial}{\partial n} G(\boldsymbol{m},\boldsymbol{l}) \right) ds \tag{8}$$

where S is the domain boundary including the wetted body surface S_W, the bubble surface S_B and the boundary S_∞ at infinity. In the equation $\boldsymbol{m}$ is the field point and $\boldsymbol{l}$ is the integral (or the source) point on the boundary. ε is the solid angle when observing the flow field at point $\boldsymbol{m}$. Green function in three-dimensional domain is $G(\boldsymbol{m},\boldsymbol{l}) = |\boldsymbol{m}-\boldsymbol{l}|^{-1}$.

Dimensionless terms are applied based on the following parameters: the typical length of the body L, the speed of the body W_∞, the density of the fluid ρ. Thus we use L/W_∞ for time, ρW_∞^2 for pressure and LW_∞ for the velocity potential respectively. The nondimensionalized parameters will then be denoted by a bar. The dimensionless boundary conditions on the body surface and the bubble surface can be given as:

$$\frac{\partial \bar{\Phi}}{\partial n} = -n_z \tag{9}$$

$$\frac{d\bar{\boldsymbol{r}}}{d\bar{t}} = \nabla \bar{\Phi} \tag{10}$$

$$\frac{d\bar{\Phi}}{d\bar{t}} = \frac{1}{2}\sigma_\infty - \frac{\lambda\sigma_\infty}{2}\left(\frac{V_0}{V}\right)^\tau + \chi\nabla\cdot\boldsymbol{n} + \frac{1}{2}|\nabla\bar{\Phi}|^2 \tag{11}$$

where n_z is the component of $\boldsymbol{n}$ in the *z*-direction, $\sigma_\infty = P_\infty / \left(\rho W_\infty^2/2\right)$ is the cavitation number, $\lambda = P_0/P_\infty$ is the strength parameter of the bubble and $\chi = \sigma/(\rho L W_\infty^2)$ is the surface tension coefficient. Hereafter, all the parameters are dimensionless and the bar is dropped for convenience.

Care must be taken at the intersections of the body surface and the bubble surface because the normal of the fluid boundary may not be continuous, although the potential itself may be. We notice that the $\partial\Phi/\partial n$ at the intersection is known if it is viewed from the element attached on the body surface, while it is unknown when it is viewed from the element attached on the bubble surface, similar to the intersection between the free surface and the body (Dommermuth & Yue, 1987[13]). Therefore, when calculating the corresponding coefficient in the matrix at the intersection, the integral can be split into two parts: one from the integration over the body surface and the other from the cavity surface. The unknown normal velocity on the intersection viewed from the cavity surface is solved together with those at the other points on the bubble surface. More details on the numerical procedure of the BEM please refer to Brebbia(1978) [14] or Ni et al.(2013)[15].

3 NUMERICAL RESULTS AND DISCUSSION

The convergence study of the procedure has been done by Ni et al.(2013)[15] as stated above, so we study the case of a bubble attached on a cylinder directly in this paper. Then the effects of the initial bubble volume on the bubble dynamics are followed.

3.1 Case study

We choose a semi-circular bubble attached on a circular cylinder with spherical ends for

the case study, as shown in Fig.2. The parameters are taken as $\sigma_\infty = 2, \lambda = 5, \chi = 10^{-4}$. The diameter of the cylinder is 1/10, and the initial profile of the bubble in the (r, z) system is a semi-circle with radius $R_0 = 1/40$. The initial distance between the centre of the bubble and the fore end of the cylinder along the z direction $L_0 = 1/4$.

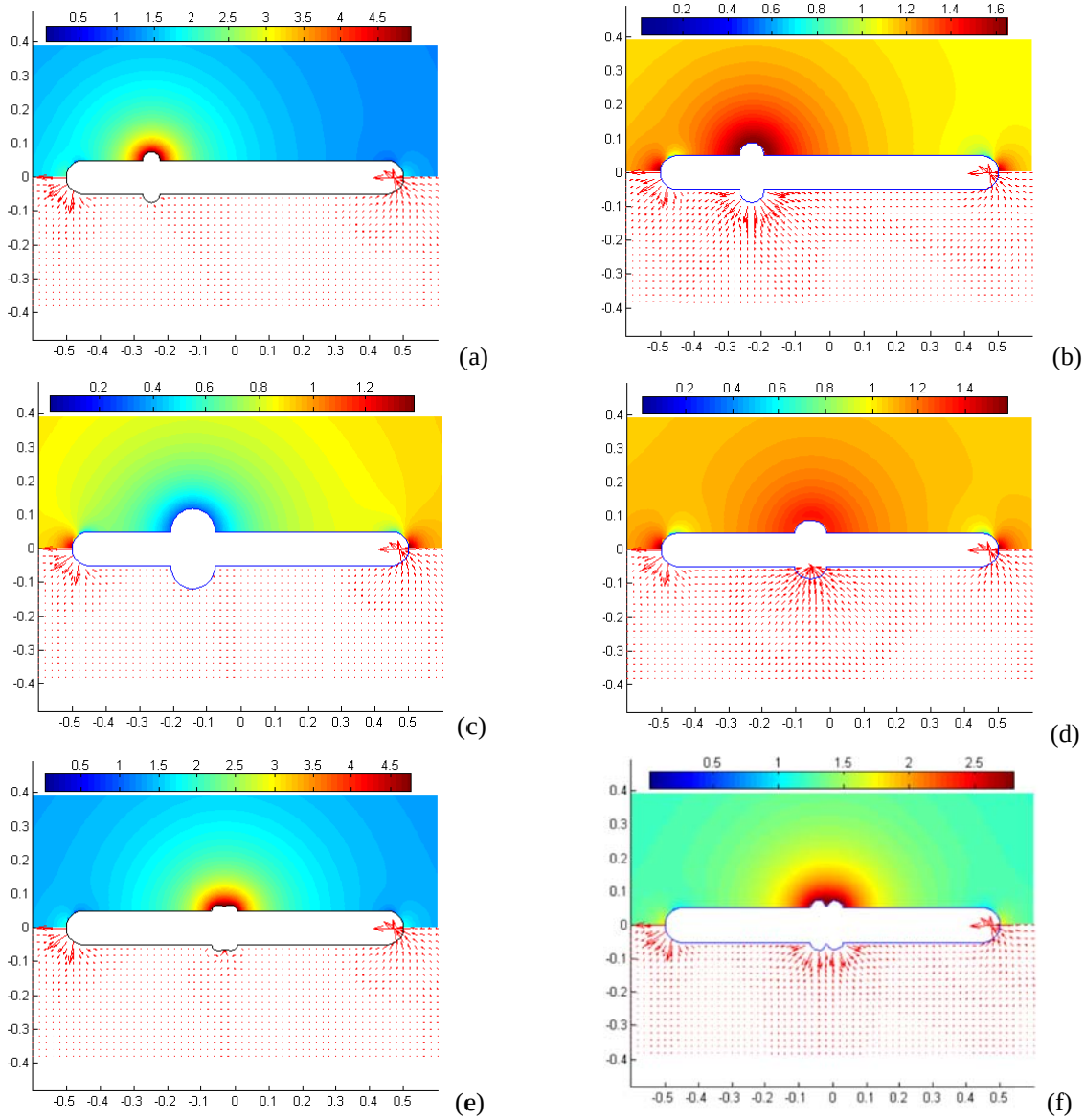

Figure 2: Velocity vectors and pressure contours for $\sigma_\infty = 2, \lambda = 5, \chi = 10^{-4}, R_0 = 1/40$. Arrow lengths are scaled with respect to maximum instantaneous velocity in each frame. The pressure scales are shown in the top half of each figure. (a) t=0 (b) $t \approx$ 0.0230 (c) $t \approx$ 0.1084 (d) $t \approx$ 0.1931 (e) $t \approx$ 0.2184 (f) $t \approx$ 0.2361 .

Fig. 2 denotes the contour of pressure and velocity around the body as well as the evolution of the bubble. Fig. 2(a) shows the initial static bubble with high pressure inside. In Fig. 2(b), the dimensionless time is t=0.0230, when the bubble expands under the motivation

of the much higher internal pressure. Fig. 2(c) shows the time when bubble volume peaks, and the bubble changes from expansion to contraction. Fig. 2(d) is the contraction stage, and it can be seen the high pressure region around the both ends of the cylinder. In Fig. 2(e), the total volume of the bubble reaches the minimum, but the particles near the middle of bubble are still moving inwards under inertia. Thus the water jet forms and 'necking' phenomenon happens. Fig. 2(f) shows the time at t=0.2361, when the jet hits the body surface and the bubble splits into two sub-bubbles. At the same time, the bubble will expands with the high pressure inside again.

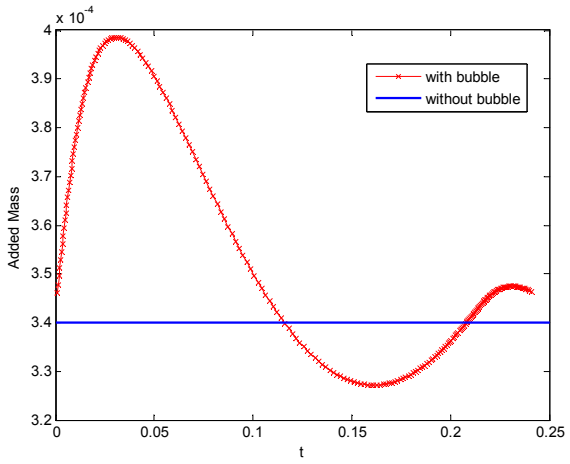

Figure 3: Variation of the added mass with time

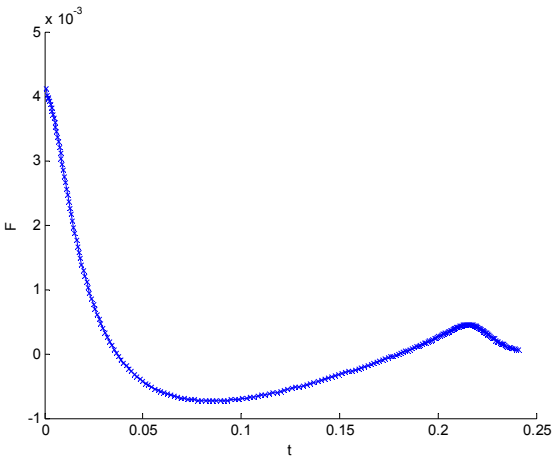

Figure 4: Variation of the force with time

Fig.3 is the time history of the added mass, in which the straight line denotes the theoretical added mass of the same cylinder without bubble attached. It shows the added mass with bubble attached fluctuates around the added mass without bubble attached along with the evolution of bubble. Fig.4 shows the time history of the force of the body, whose direction is opposite to the moving direction. There are two methods to calculate the force: one is the integral method, which just integrates the pressure on the body surface. The other one is differential method, which is obtained by $F_{zz} = \frac{d(m_{zz} \cdot W_\infty)}{dt} = \frac{dm_{zz}}{dt} W_\infty + m_{zz} \frac{dW_\infty}{dt} = \frac{dm_{zz}}{dt}$. Numerical calculation has validated that the results of these two methods coincides. Here we just adopted the second method because the added mass has been calculated in Fig.3. It can be seen in Fig.4. that the pressure of the fore half is greater than that of rear half and the resultant force points backwards, as the high pressure bubble released on the foreside of the body. After that, the force changes its direction and quantity along with the evolution of bubble pressure.

Fig.5 represents the time history of the gas pressure P_b inside the bubble, while Fig.6 shows the change of the bubble jet velocity V_{jet}, which is defined as the fluid velocity along the r axis at the bubble midpoint. It can be seen form these curves that the jet velocity V_{jet} peaks and the pressure P_b approaches to 1 around t=0.023, before P_b reaches bottom and V_{jet} reduces to zero around t=0.108. Then V_{jet} hits the bottom around t=0.204, which means the contracting velocity at the bubble midpoint is maximum, while P_b peaks again around

t=0.218, which corresponds to the minimum bubble volume in Fig.2 (e). At last V_{jet} is rough –0.15, which denotes that the water hits the body surface with a dimensionless velocity of 0.15 roughly.

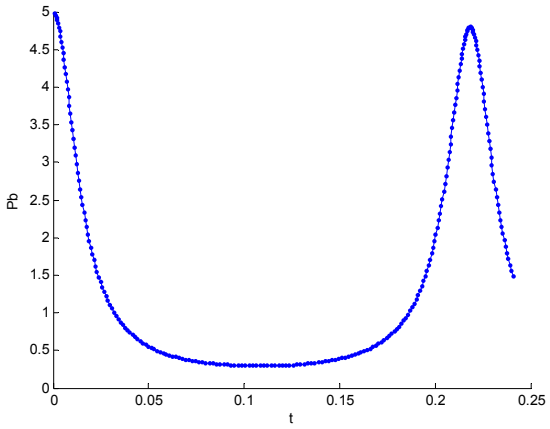

Figure 5: Variation of the gas pressure inside the bubble with time

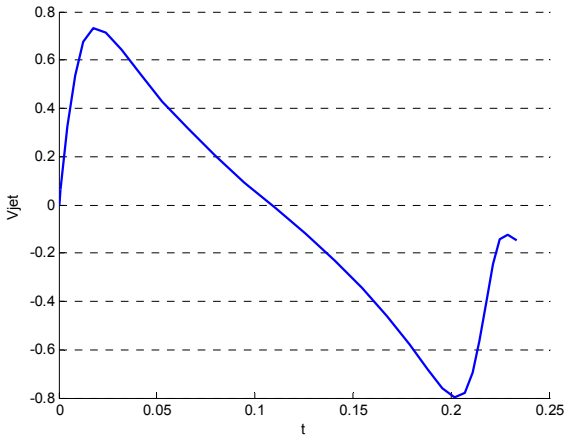

Figure 6: Variation of the bubble jet velocity with time

3.2 Influence of initial bubble volume

To study the influence of the initial volume on bubble dynamics, we take $R_0 = 1/40$ and $R_0 = 1/400$ as examples and other parameters are $\sigma_\infty = 8, \lambda = 5, \chi = 10^{-4}, L_0 = 1/2$ .The evolution of bubbles are shown in Fig.7.

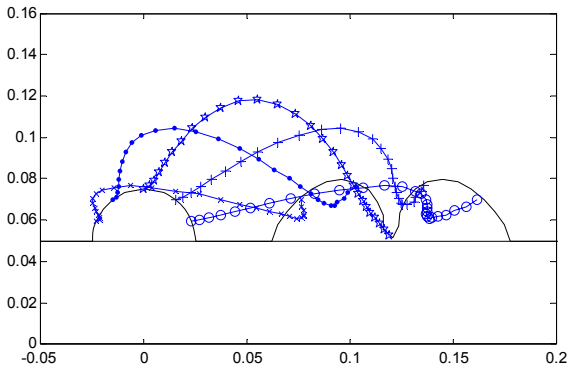

(a)

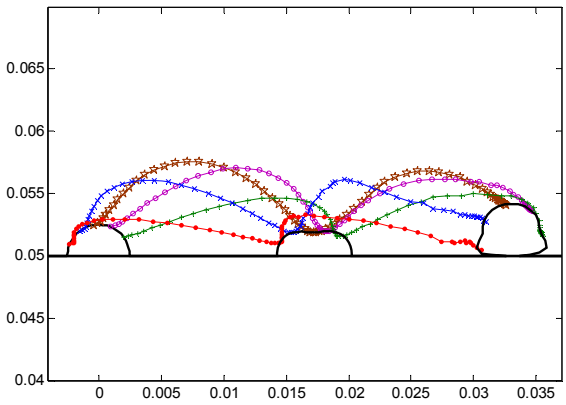

(b)

Figure 7: Effect of initial volume of bubble, the tracks of fluid particles during the evolution of bubble of (a) $R_0 = 1/40$ (b) $R_0 = 1/400$ with $\sigma_\infty = 8, \lambda = 5, \chi = 10^{-4}, L_0 = 1/2$.

From Fig.7 (a), we can see that a jet forms at the first contraction stage for $R_0 = 1/40$ when λ=5. In contrast, there is no formation of a jet for the bubble with initial radius $R_0 = 1/400$ in

Fig.7 (b). From the movement of the fluid particles for $R_0 = 1/400$, we can see that the middle part of bubble surface is flattened when bubble reaches its first minimum volume, before the bubble expands and starts the second phase of oscillation.

One main reason why the smaller bubble would not form a jet in the first oscillation may be the effect of surface tension. According to the Young-Laplace equation, the local curvature can be written as $\nabla \cdot \boldsymbol{n} = 1/R_1 + 1/R_2$, where R_1 and R_2 are corresponding principal radii of curvature. So $\nabla \cdot \boldsymbol{n}$ gets large as the initial bubble radius R_0 (namely the R_1 in the equation) reduces. Because the dimensional surface tension coefficient σ is quite small, for example $\sigma = 0.078\mathrm{N/m}^2$ for water of $20^{\circ}\mathrm{C}$, the surface tension will have a small contribution to Eq.(6) if R_0 is large. However, the effect of surface tension becomes more important as R_0 decreases. To further support this statement, simulation is made under the same condition with Fig. 7(b) but at χ=0. The results are shown in Fig.8. It can be seen a jet pointing towards the body surface would form, when the surface tension is not taken into account under the same condition.

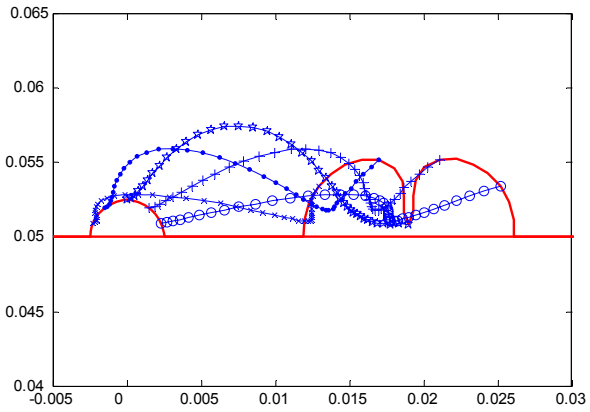

Figure 11: The tracks of fluid particles during the evolution of bubble of $R_0 = 1/400$, with $\sigma_\infty = 8, \lambda = 5, \chi = 0, L_0 = 0.5$.

4 CONCLUSIONS

- The evolution and dynamics of the bubble itself depends strongly on the combined effects of the initial bubble pressure, surface tension and the ambient pressure. For a given ambient pressure, whether the bubble initially expands or contracts would depend on the specific combination of the initial pressure and surface tension.
- When the initial pressure is much higher than the ambient pressure, a bubble jet will form during the contraction and a bubble will split into two sub-bubbles. Various results such as force and added mass of the body depend strongly on the evolution and position of the bubble.
- As the initial bubble radius decreases, the surface tension plays a more and more important role in the evolution of bubble, which tends to sustain the bubble in a stable shape longer.

ACKNOWLEDGEMENTS

This work is supported by Lloyd's Register Foundation through the joint centre involving University College London, Shanghai Jiaotong University and Harbin Engineering University and the National Natural Science Foundation of China (No. 11302056 and No. 11302057) China Postdoctoral Science Foundation(No. 2013M540272), to which the authors are most grateful. Lloyd's Register Foundation, a UK registered charity and sole shareholder of Lloyd's Register Group Ltd, invests in science, engineering and technology for public benefit, worldwide.

REFERENCES

[1] Cerrio S.L. Friction Drag Reduction of External Flows with Bubble and Gas Injection, *Annual Review Fluid Mechanics*. 2010, 42:183-203

[2] McCormick M E, Bhattacharya R. Drag reduction of a submersible hull by electrolysis. *Naval Engineers Journal*，1973, 85:11-16

[3] Latorre, R., Ship hull drag reduction using bottom air injection, *Ocean Engineering*, 1997, 24 (2):161-175.

[4] Legner H H．A simple model for gas bubble drag reduction. *Physics of Fluids*，1984，27 (12): 2788-2790

[5] Madavan N K，Deutscb S， Merkle C L. Measurements of local skin friction in a microbubble-modified turbulent boundary layer, *Journal of Fluid Mechanics*, 1985, 156:237-256

[6] Brokett T.. Computational method for determination of bubble distributions in liquids[R]. [S.l.]: U. S. Naval Ship Research Development Cenret, 1969.

[7] Drew D A.. Mathematical modeling of two-phase flow. *Annual Review of Fluid Mechanics*, 1983, 15: 261-291.

[8] Matveev, K.I., Modeling of vertical plane motion of an air cavity ship in waves, *Fifth International Conference on Fast Sea Transportation*, FAST, Seattle, USA, 1999

[9] Matveev K.I., Burnett T.J., Ockfen A.E.. Study of air-ventilated cavity under model hull on water surface. *Ocean Engineering*, 2009, (36):930-940

[10] Li Y.B., Wu X.Y., Ma Y. Wang J.G.. A method based on potential theory for calculating air cavity formation of an air cavity resistance reduction ship, *Journal of Marine Science Application*. 2008, 7:98-101

[11] Choi, J.K., Hsiao, C.T., Chahine, G. L., Design trade-off analysis for high performance ship hull with air plenums, *Proc. 2nd International Symposium on Seawater Drag Reduction*, Busan, Korea, 2005.

[12] Choi, J.K., Chahine, G. L.. Numerical Study on the Behavior of Air Layers Used for Drag Reduction. *28th Symposium on Naval Hydrodynamics*, Pasadena, California, 2010

[13] Dommermuth, D., Yue, D.K.P., Numerical simulations of nonlinear axisymmetric flows with a free surface, *Journal of Fluid Mechanics*, 1987, 178: 195-219

[14] Brebbia C.A., 1978, *The boundary element method for engineers*. London : Pentech Press , London, UK.

[15] Ni B.Y. Zhang A. M., Wu G.X., Numerical simulation of motion and deformation of ring bubble along body surface, *Applied Mathematics and Mechanics*,2013,34(12):1495-1512.